JACS
JOURNAL OF THE AMERICAN CHEMICAL SOCIETY
Article
pubs.acs.org/JACS

Controlling Solid–Gas Reactions at Nanoscale for Enhanced Thin Film Morphologies and Device Performances in Solution-Processed $Cu_2ZnSn(S,Se)_4$ Solar Cells

Chengyang Jiang,[†,‡] Yao-Tsung Hsieh,[†,‡] Hongxiang Zhao,[†,‡] Huanping Zhou,[†,‡] and Yang Yang*[,†,‡]

[†]Department of Materials Science and Engineering and [‡]California NanoSystems Institute, University of California, Los Angeles, California 90095, United States

Supporting Information

ABSTRACT: Using $Cu_2ZnSn(S,Se)_4$ (CZTSSe) as a model system, we demonstrate the kinetic control of solid–gas reactions at nanoscale by manipulating the surface chemistry of both sol–gel nanoparticles (NPs) and colloidal nanocrystals (NCs). Specifically, we first identify that thiourea (commonly used as sulfur source in sol–gel processes for metal sulfides) can transform into melamine upon film formation, which serves as surface ligands for as-formed Cu_2ZnSnS_4 (CZTS) NPs. We further reveal that the presence of these surface ligands can significantly affect the outcome of the solid–gas reactions, which enables us to effectively control the selenization process during the fabrication of CZTSSe solar cells and achieve optimal film morphologies (continuous large grains) by fine-tuning the amount of surface ligands used. Such enhancement leads to better light absorption and allows us to achieve 6.5% efficiency from CZTSSe solar cells processed via a sol–gel process using nontoxic, low boiling point mixed solvents. We believe our discovery that the ligand of particulate precursors can significantly affect solid–gas reactions is universal to solid-state chemistry and will boost further research in both understanding the fundamentals of solid-state reactions at nanoscale and taking advantage of these reactions to fabricate crystalline thin film semiconductors with better morphologies and performances.

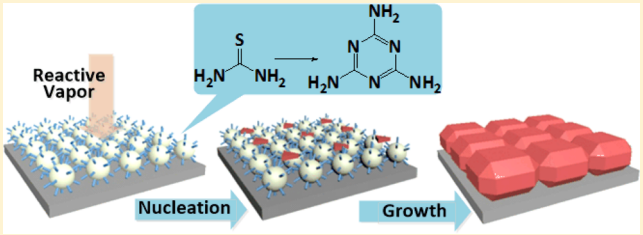

INTRODUCTION

Bottom-up fabrication of inorganic semiconductor materials via solution-based processes has been intensively investigated in recent years[1,2] due to its low capital and operational costs, compatibility with roll-to-roll manufacture (and even 3D printing), and mild processing conditions that expand the list of available substrates, including flexible ones. Particularly, the applications of thin film materials fabricated via solution process have been actively assessed in the field of various electronics and optoelectronics, including but not limited to field-effect transistors,[3−5] transparent conductive electrodes,[6,7] memory devices,[8,9] light-emitting diodes,[10,11] photodetectors[5,12] and solar cells.[13−15]

A key aspect in solution-processing of inorganic materials is the design of precursor solutions ("inks"). Two types of precursor solutes, namely molecular species and colloidal nanocrystals (NCs), are typically adopted to form the inks. The former one undergoes sol–gel processes that lead to the in situ formation of nanoparticles (NPs) with desired compositions and phases,[16] while the latter one usually contains NCs with same composition as the target phase, although rationally designed NCs that can be subsequently transformed into target phases have also been demonstrated.[17] For both sol–gel processes and colloidal NC routes, nanoscale building blocks are fundamental to the fabrication of crystalline films.

In order to maintain the solubility and stability of the inks, both molecular species and colloidal NCs require surface ligands linking to the metal ions. The ligands in molecular solutions usually refer to small anionic species, while in NCs ligands refer to the surfactants that cap the NC surfaces. These ligands typically represent undesired impurities or even dopants that should be eliminated via thermal treatment in ideal cases. For NCs, the understanding of ligand chemistry and the ability to manipulate ligands have improved a lot over the past few years.[18] In molecular inks, however, due to higher complexity of sol–gel processes, how ligands affect phase formation and eventually device performances is still largely unexplored.

As the solution process of inorganic thin film semiconductors naturally satisfy several requirements posed in thin film compound solar cells, such as small and controllable thicknesses, low fabrication costs, and compatibility with high-throughput processes, the study of solution-processed thin film solar cells has been a constant focus of research,[19] with target materials include almost all commercialized and emerging techniques including CdTe,[20,21] $Cu(In,Ga)Se_2$ (CIGS),[22,23] $Cu_2ZnSn(S,Se)_4$ (CZTSSe),[24,25] $Sb_2(S,Se)_3$[26,27] and quantum dot solar cells.[14,28] Among these materials, CZTSSe is particularly attractive due to its similarities to the technologically successful CIGS, involvement of only cheap, earth-abundant and nontoxic elements, and more importantly,

Received: June 5, 2015
Published: August 17, 2015

DOI: 10.1021/jacs.5b05819
J. Am. Chem. Soc. 2015, 137, 11069−11075

demonstrated record power conversion efficiency (PCE) of 12.7% via a solution-based process.[29]

As mentioned before, the incorporation and understanding of surface ligands are important topics for solution-processed inorganic semiconductors, and CZTSSe is no exception. Unfortunately, although the solution-based fabrication of CZTSSe via both sol−gel processes and NC inks have been extensively explored, understanding of the role of ligands in both scenarios is largely limited. This is partially because the postdeposition annealing in selenium atmosphere, so-called "selenization", incurs further chemical complications[30] and makes it difficult to reveal the actual roles ligands play in the entire course. For NC inks, researchers have observed that surface ligands significantly affect the outcomes of the selenization in terms of grain formation,[31] and have proposed a variety of ligand exchange pathways to modify the NC surfaces.[25,32−34] In sol−gel processes, due to the fact that more chemical species and reactions are entangled, it becomes even harder to define and find out the actual ligand species, if any, that plays a role in the selenization process.

In this contribution, we demonstrate that in a sol−gel process for CZTSSe solar cells, the ligands formed in situ will significantly affect the surface chemistry of NPs synthesized during deposition, and thus the kinetics of selenization process and eventually the crystalline grain morphologies. We also prove that we can effectively control such surface chemistry via tuning the amount of ligands, which enables us to enhance the film formation and the performances of solar cells. We believe our discoveries are general to the fabrication of inorganic crystalline materials adopting solution-based processes.

EXPERIMENTAL SECTION

Chemicals. Copper(II) acetate monohydrate ($Cu(OAc)_2·H_2O$, 99.0%, Aldrich), tin(II) chloride dihydrate ($SnCl_2·2H_2O$, 98%, Aldrich), zinc acetate dihydrate ($Zn(OAc)_2·2H_2O$, 98%, Aldrich), thiourea (99.0%, Aldrich), methanol (MeOH, 99.9%, Fisher), 2-methoxyethanol (2-ME, 99.9%, Aldrich); selenium shots (99.999%, Alfa Aesar); Cadmium acetate dihydrate ($Cd(OAc)_2·2H_2O$, 98%, Aldrich), ammonium acetate (NH_4OAc, 99.999%, Aldrich), ammonium hydroxide ($NH_3·H_2O$, 28−30%), deionized water (DIW, 18 MΩ); Oleylamine (OAm, 70%, Aldrich), toluene (99.5%, Macron), ethanol (EtOH, 200 proof, Decon Laboratories).

Preparation of Molecular Inks. 3.52 mmol $Cu(OAc)_2·H_2O$ was dispersed into the mixture of 4 mL of MeOH and 4 mL of 2-ME. Then, 2.24 mmol $SnCl_2·2H_2O$ was added, which incurs an immediate redox reaction that changes the color of the suspension from greenish blue to white. After sonication of the suspension, 2.40 mmol $Zn(OAc)_2·2H_2O$ and selected amount (8.80, 9.90, 11.0, 12.1, or 13.2 mmol) of thiourea were introduced, leading to the formation of a transparent, colorless to pale yellow solution.

Deposition of Precursor Films. Two mL of precursor solution was diluted with 0.5 mL of MeOH and 0.5 mL of 2-ME prior to deposition. In a nitrogen-filled glovebox, one drop of solution was spin-cast onto the surface of molybdenum-coated glass (purchased from Thin Film Devices Inc.) at 3000 rpm for 30 s, followed by curing of the film first at 300 °C on a hot plate for 2 min, then at 400 °C in a muffle furnace for 3 min (hereafter referred to as "high-temperature curing"). The next layer was coated in the same manner except that the film was cured at 300 °C for 5 min (hereafter referred to as "low-temperature curing"). Such processes were then performed alternatively until desired thickness (verified by surface profilometry) was achieved. Typically 6−8 layers of solution were coated onto the substrate.

Preparation of NC Precursor Films. Colloidal syntheses and film deposition were performed according to established methods.[35] CZTS NCs with extra ligands were prepared by adding 100 μL of OAm to 1 mL of colloidal CZTS stock solution, heating, sonicating and stirring the solution for several days to ensure complete ligand capping. CZTS NCs with reduced amount of ligands were prepared by adding 3 mL of EtOH to 1 mL of stock solution to flocculate, centrifuging at 10 000 rpm for 10 min, collecting and redispersing precipitates in 1 mL of toluene.

Device Fabrication. As-deposited precursor films were placed in a graphite box together with 1 Se shot (ca. 50 mg) per film. The graphite box was inserted into a muffle furnace or tube furnace preheated to 540−560 °C and kept for 15−30 min before the door of muffle furnace was opened or the tube of tube furnace was hoisted to allow natural cooling. This process is further referred to as "selenization". Selenized samples were coated with CdS emitter using chemical bath deposition (the bath contains 190 mL of DIW, 138 mg of $Cd(OAc)_2·2H_2O$, 4 mL of 1 M NH_4OAc (aq.), 6 mL of $NH_3·H_2O$ and 2 mL of 0.5 M thiourea (aq.) and the reaction is held at 65 °C for 25−30 min) and In_2O_3:Sn (ITO) top electrode using the sputtering system from ULVAC. Lastly, the finished devices were mechanically scribed into 3 mm × 4 mm areas and indium dots were stuck to both front and back contacts to facilitate charge collection.

Solid-State Nuclear Magnetic Resonance (SSNMR) Spectroscopy. In a nitrogen-filled glovebox, the CZTS precursor solution, or 2.75 mmol thiourea dissolved in the mixture of 1 mL of MeOH and 1 mL of 2-ME, was first drop-casted onto a large piece of slide glass and heated first at 300 °C for 2 min then at 400 °C for 3 min. Resembling "high-temperature curing", this procedure was repeated for 3 times to collect enough material. The final film was scraped off the substrate and resultant loose powder was collected and pumped under vacuum overnight to remove any moisture. For measurements, 4 mm cross-polarization/magic angle spinning (CP/MAS) probe was used and rotor containing the sample (mixed with NaCl to fill rotor if necessary) was loaded into Bruker Avance DSX 300 MHz SSNMR spectrometer. ^{13}C signals were referenced to trimethylsilane (TMS). Spinning frequency was 10 kHz and recycle delay was 15 s (300 s recycle delay did not give extra signals).

X-ray Fluorescence (XRF) Spectroscopy. Bulk compositions of precursor and selenized films were measured using Rigaku Supermini 2000 XRF spectrometer.

Powder X-ray Diffractometry (XRD). Diffraction patterns of precursor films and selenized films were measured using PANalytical X-Pert Pro X-ray powder diffractometer with Cu Kα radiation. Narrower slit and smaller step size were used for better angular resolution.

Raman Spectroscopy. Raman spectra of precursor and selenized films were measured using Renishaw inVia Raman microscope with 633 nm laser.

Scanning Electron Microscopy (SEM). SEM images of selenized films were taken using FEI Nova NanoSEM 230.

Current−Voltage (*I*−*V*) Measurement. Performances of CZTSSe solar cells were measured using Keithley 2400 SourceMeter and Newport Oriel 92192 solar simulator under an AM1.5G filter at 100 mW/cm^2.

External Quantum Efficiency (EQE) Measurement. Quantum efficiencies of CZTSSe devices were measured using Enlitech QE-R system at 0 or −0.5 V bias.

RESULTS AND DISCUSSION

The sol−gel process in this work is based on the molecular ink containing all constituents for Cu_2ZnSnS_4 (CZTS), namely copper(II) acetate ($Cu(OAc)_2·H_2O$), zinc acetate ($Zn(OAc)_2·H_2O$), tin(II) chloride ($SnCl_2·2H_2O$) and thiourea ($CS(NH_2)_2$). All of these species are cheap, nontoxic and commercially available. More importantly, minimizing the use of chloride reduces undesired *n*-type doping and prevents the loss of Sn during film deposition presumably via inhibiting the formation and evaporation of $SnCl_4$ (whose boiling point is only 114 °C), thus ensuring better atom economy and control over film stoichiometry (see Figure S1 for the drastic

DOI: 10.1021/jacs.5b05819
J. Am. Chem. Soc. 2015, 137, 11069−11075

stoichiometric change when chlorides are used for all three metals, as verified by XRF). The 1:1 mixture of methanol (MeOH) and 2-methoxyethanol (2-ME) is used as the solvent to provide both solubility and stability of the constituents. Control experiments show that pure MeOH or the mixture of ethanol and 2-ME cannot fully dissolve the aforementioned species (Figure S2) while pure 2-ME[36] results in the formation of brown precipitates (presumably Cu_2S). Moreover, mixed solvents are frequently used in thin film deposition of polymeric materials[37] and nanocrystal superlattices[38] with the advantage of achieving more uniform coatings.

The as-synthesized molecular ink is a colorless to pale yellow solution (Figure S2) and can be stored in ambient atmosphere without any degradation given that enough thiourea is added. Such phenomenon indicates that thiourea serves as ligands to metal cations via the formation of metal−sulfur bonds, as is proven in previous studies.[39,40] Upon deposition and heat treatment, these metal-thiourea complexes transform into binary, ternary and eventually quaternary chalcogenide species (i.e., CZTS) in form of NPs. XRD patterns (Figure S3) and Raman spectra (Figure S4) prove the formation of CZTS phase with small crystal sizes at this stage. Interesting question raised here is whether there are any ligands capping the surfaces of NPs synthesized via sol−gel processes as in the case for colloidal NCs, and if so, how these capping ligands are related to thiourea (which serves as the ligand in molecular inks[36]). Such questions are fundamentally important for any sol−gel processed inorganic semiconductors, as the existence of these ligands can significantly affect the charge transport behaviors of the films. This issue is particularly imminent in solution processed CZTSSe, as it has already been proven that the outcomes of the selenization process (in terms of the formation of crystalline films comprising large grains) are largely subject to the existence and chemical species of the surfaces ligands to colloidal NCs,[31] and the same should also apply to NPs formed in situ during sol−gel processes.

Although previous report has suggested that excess thiourea used in sol−gel processes can be fully removed through the formation of volatile species upon heat treatment,[41] further studies demonstrate that it can actually leave behind residues even at very high temperatures.[42,43] As a matter of fact, it is documented that depending on the temperature, duration and atmosphere provided, thiourea undergoes a series of reactions, including transformation, decomposition and condensation (Scheme 1).[43−45]

Particularly, reaction (2) reveals one key nonvoltaile compound from the direct decomposition of thiourea, namely cyanamide (CH_2CN), which can polymerize into dimer (2-cyanoguanidine) and trimer (melamine) at elevated temperatures through reactions (5) and (6) respectively. Moreover, melamine can undergo further condensation and give rise to melam and melem according to reactions (7) and (8). Melem molecules can again link through the loss of NH_3 and form melon ($(C_6N_9H_3)_x$) and eventually graphitic carbon nitride (g-C_3N_4, reactions not shown here).[46]

Such rich chemistry of thiourea transformation leads to the hypothesis that some of the aforementioned nonvolatile species may actually form during our sol−gel process and serve as surface ligands for CZTS NPs formed in situ. Therefore, we took advantage of ^{13}C solid-state nuclear magnetic resonance spectroscopy (^{13}C-SSNMR) to detect the formation of thiourea derivatives (see Experimental Section for details). Two reasons determine the choice of ^{13}C-SSNMR over routine liquid-phase ^{1}H NMR. One is that many aforementioned species share peaks at similar positions in ^{1}H NMR (ca. 7.3 ppm and ca. 6.0 ppm) and thus cannot be distinguished. The other reason is that many thiourea derivatives with higher molecular weights (such as melamine and melem) cannot be fully dissolved even in dimethyl sulfoxide (DMSO), which may lead to preferential uptake of certain species and cause misleading interpretation of reactions.[45] For ^{13}C-SSNMR, besides black CZTS powders extracted from the sol−gel process, samples from pure thiourea dissolved in the mixture of MeOH and 2-ME were also prepared in the same manner and used for comparison. Interestingly, we find that even after high-speed centrifugation, the black powder containing as-formed CZTS NPs can still be partially redispersed in DMSO, strongly suggesting that these NPs are actually capped with surface ligands and are therefore colloidally stable in suitable solvents.

^{13}C-SSNMR spectra of samples derived from thiourea and molecular ink show similar features, with a characteristic peak at 164 ppm (Figure 1). For thiourea derivatives, another weaker peak at 156 ppm is also observed, and it manifests itself as a hump in sol−gel CZTS derivatives. The absence of peaks at 184 or 134 ppm indicates that all pristine thiourea and thiocyanate (such as guanidinium thiocyanate from reaction (4)) are no longer present and have probably been transformed to oligomeric species.[44,47] Previous study has revealed that the peak at 164 ppm indicates the presence of a triazine ring in which the carbon bonds with a -NH_2 group, while the peak at 156 ppm indicates that the carbon bonds with a -NH- group.[44] Pursuant to such identification and comparison of our results with published spectra,[45,48,49] we can conclude that under our conditions for thin film fabrication, pure thiourea is transformed into either melem or adducts related to melem,[45] both

Scheme 1. Transformations of Thiourea at Elevated Temperatures under Inert Atmosphere

$$CS(NH_2)_2\ (\text{thiourea}) \rightarrow NH_4SCN \quad (1)$$

$$2CS(NH_2)_2 \rightarrow CS_2\uparrow + 2NH_3\uparrow + NH_2CN\ (\text{cyanamide}) \quad (2)$$

$$NH_4SCN \rightarrow NH_3\uparrow + HNCS\uparrow\ (\text{isothiocyanic acid}) \quad (3)$$

$$CH_2CN + NH_4SCN \rightarrow [C(NH_2)_3]SCN \quad (4)$$

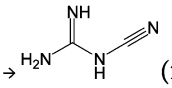

(5)

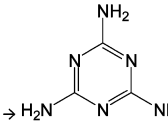

(6)

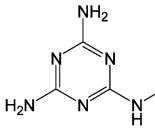

(7)

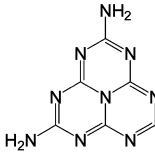

(8)

DOI: 10.1021/jacs.5b05819
J. Am. Chem. Soc. 2015, 137, 11069−11075

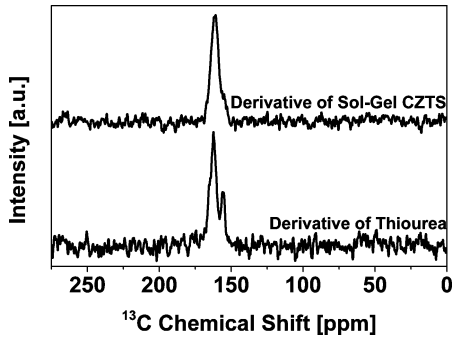

Figure 1. ^{13}C CP-MAS SSNMR spectra (referenced to TMS) of derivatives of thiourea and CZTS molecular ink.

of which have carbons with two distinct chemical environment and thus show two peaks in ^{13}C-SSNMR spectra. While for sol–gel CZTS, most of the contained thiourea is only transformed to melamine with one type of carbon whose chemical shift is around 164 ppm.[48,49] The formation of oligomeric compounds such as melamine and melem is also supported by the fact that the color of thiourea samples changed gradually from white to beige upon heating, which suggests that large conjugated molecules absorbing visible light have formed in this process.

As it is elucidated that thiourea in the molecular inks transform into nonvolatile species (mostly melamine) which may serve as surface ligands for as-formed CZTS NPs and affect their reactions with Se vapor, we set out to prepare a series of inks with various thiourea concentrations (the molar ratios between thiourea and total metal ions are set to be 1.08, 1.21, 1.35, 1.48, and 1.62 to form a series) and deposited these inks on glass substrates coated with 750 nm molybdenum which were subject to high-temperature heat treatment under selenium atmosphere. A special two-step heat treatment for film curing is invented in this work to release film stress and eliminate film cracks (see Experimental Section and Figure S5 for details). After selenization, dramatic differences are seen from SEM images for samples with varying amount of thiourea (Figure 2). At thiourea to metal ratio ([tu]/[M]) of 1.08 (Figure 2A), compact but relatively small grains of CZTSSe form upon selenization, and the sizes of grains gradually increase as the ratio increases to 1.21 (Figure 2B) and 1.35 (Figure 2C). However, when the ratio is further increased to 1.48 (Figure 2D), although even larger grains adjacent to each other are observed, areas without large grains can clearly be observed, and such trend continues as the ratio reaches 1.62 (Figure 2E), the highest used in this study, in which scenario colossal grains up to 5 μm scatter scarcely on top of a small-grain layer. We have also measured the diameters of over 100 grains in each sample and calculated their average sizes to confirm such trend (Figure 2F). Besides, Raman spectra and XRD patterns both prove that large grains are pure CZTSSe phase in all scenarios (Figure S6 and S7). These sets of experiments unambiguously show that thiourea derivatives play a key role in manipulating the kinetics of the selenization process.

The underlying mechanisms of selenization (or sulfurization) are becoming increasingly clear thanks to the efforts from several research groups.[30,31,50−52] It has now been experimentally observed that at least three processes occur during the course of selenization. The first one is the downward diffusion and incorporation of Se as well as the upward

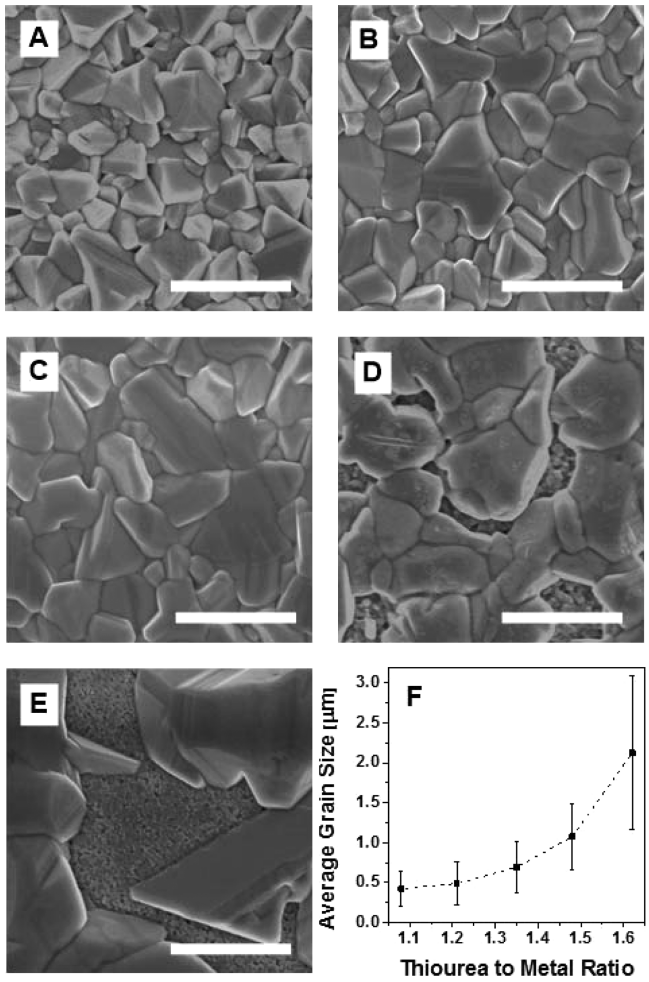

Figure 2. (A–E) SEM images of selenized CZTSSe films with [tu]/[M] equal to (A) 1.08, (B) 1.21, (C) 1.35, (D) 1.48 or (E) 1.62 (scale bar = 2 μm). (F) Changes of average grain sizes (measured from over 100 grains for each sample) with respect to the changes of [tu]/[M].

diffusion and removal of S, which leads to the formation of CZTSSe in replacement of CZTS, independent of any sintering or solid-state reactions.[53] The diffusion of Se also causes the oxidation of Mo contact and results in the formation of $MoSe_2$ layer.[54] The second process is the sintering of small colloidal CZTS NCs or CZTS NPs derived from the sol–gel process. The outcomes of the sintering process depend on the sizes and surfaces of as-deposited particles.[33] For CZTSSe, sufficient sintering of particles which leads to large grains at micrometer scale is usually not possible[33] due to inadequate energy supply during normal conditions used in selenization, while higher temperature and longer time cannot be applied because CZTSSe partially decomposes due to the volatility of SnSe beyond 450 °C. Consequently, the sintering of CZTS particles, although ubiquitous during selenization, does not contribute to the formation of desired absorbing layers. The third and most important process occurred during selenization is the solid–gas reaction between the CZTS precursor film and the Se vapor which eventually results in the formation of optoelectronically active layers composed of CZTSSe large grains. Both in situ and ex situ experiments have revealed that this reaction initiates with the reaction between Cu^+ and Se vapor which leads to the formation of Cu_xSe crystals on top of the precursor film.[30,50] This reaction is followed by the upward diffusion and

DOI: 10.1021/jacs.5b05819
J. Am. Chem. Soc. 2015, 137, 11069−11075

incorporation of Sn^{4+} ions to form Cu_2SnSe_3 (or Cu_3SnSe_4 as revealed in a recent study[31]), which further reacts with the less mobile Zn^{2+} ions to form CZTSe grains.

Solid−gas reactions, as exemplified by the reaction between CZTS particles and Se vapor, are not well studied and understood in general. However, theories of crystal nucleation and growth widely used in solid-state chemistry still apply here (Scheme 2). In this particular system, the heterogeneous

Scheme 2. Illustration of How Surface Chemistry of NPs Affects the Kinetics of Solid−Gas Reactions and Final Grain Sizes

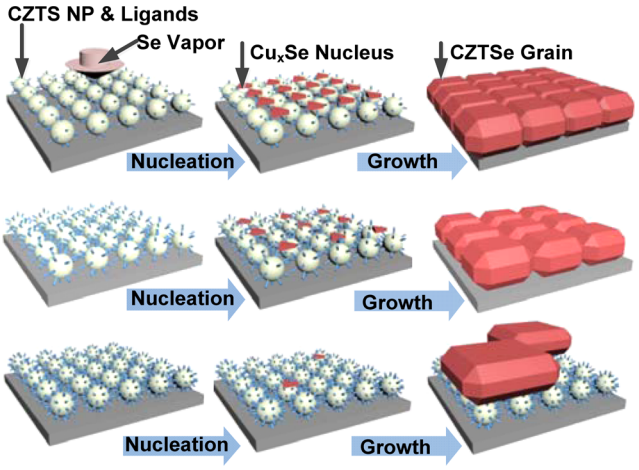

nucleation at the solid−gas interface, which leads to the formation of Cu_xSe, represents the highest energy barrier in the entire reaction, while the subsequent diffusion-controlled overgrowth of the nuclei (i.e., incorporation of Sn^{4+} and Zn^{2+}) is kinetically more favorable. (And this is why intermediate phases such as Cu_2SnSe_3 are not usually observed.) Our results clearly demonstrate that the kinetics of nucleation can be effectively manipulated by changing the surface chemistry of CZTS NPs via tuning the amount of thiourea used. As [tu]/[M] increases from 1.08 to 1.21 and to 1.35, the kinetics of nucleation become more and more sluggish, meaning less and less nuclei form at the solid−gas interface. Highest density of nuclei at ratio equal to 1.08 implies that the overgrowth of nuclei will only lead to smaller grains because adjacent grains will be in contact with each other and further overgrowth is thus inhibited (Scheme 2, top row). As the density of nuclei decreases, each nucleus is farther away from its nearest neighbor, which results in less restricted overgrowth and eventually larger grains (Scheme 2, middle row). On the other hand, when the ratio further increases from 1.35 to 1.48, the nucleation becomes too retarded that there are only a few nucleation sites on the film, and as a result, even final grains are not closely packed (Scheme 2, bottom row). It is worth mentioning that at this point, the kinetics of overgrowth is also slower than in previous cases because excess melamine can also decelerate the diffusion of Sn^{4+} and Zn^{2+} ions. Such effect is even more obvious when the ratio reaches 1.62, in which scenario much inhibited nucleation eventually brings about the formation of highly scattered large grains. These contrasts caused by the differences in kinetics are even more dramatic when lower selenization temperature and shorter selenization time are used (Figure S8).

Controlling the sizes of crystalline grains is a key topic for thin film technologies based on inorganic semiconductors, since the grain boundaries are usually trap states that jeopardize charge transport, or scattering centers that disrupt light absorption. Here we have shown that by controlling the kinetics of solid−gas reactions, especially the nucleation step, via fine-tuning the surface chemistry of NP reactants, we are able to find a balance between grain sizes and grain continuity which is optimal for charge transport. We further fabricated CZTSSe solar cells using normal device architectures to demonstrate the differences of device performances resulted from the variation in film morphologies (Figure 3A, Table 1

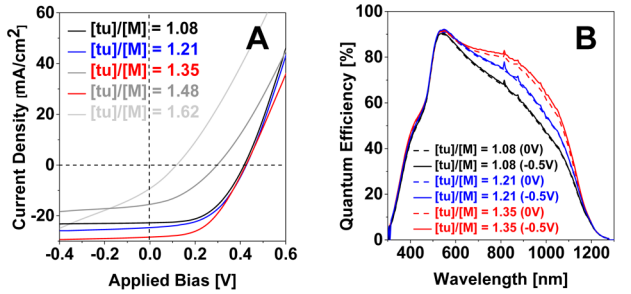

Figure 3. (A) Current−voltage characteristics of CZTSSe solar cells fabricated from precursors with varying [tu]/[M]. (B) EQE spectra of corresponding devices.

Table 1. Device Characteristics of a Typical Set of CZTSSe Cells with Various Amount of Thiourea in the Precursors

[tu]/[M]	V_{OC} (V)	J_{SC} (mA/cm^2)	FF (%)	PCE (%)
1.08	0.417	22.74	51.18	4.85
1.21	0.426	24.63	49.97	5.24
1.35	0.424	28.40	49.11	5.92
1.48	0.296	15.55	36.77	1.69
1.62	0.118	9.22	28.33	0.31

and Table S1). As expected, at [tu]/[M] equal to 1.48 and 1.62, solar cells suffer from serious shunting due to incomplete formation of large-grain layers (Figure 3A, dark gray and light gray curves). On the other hand, at [tu]/[M] equal to 1.08, 1.21 and 1.35, devices show much better power conversion efficiency (PCE) which increases as grains become larger (Figure 3A, black, blue and red curves). Interestingly, such enhancement in performance is resultant from the increase in short circuit current (J_{SC}) rather than open circuit voltage (V_{OC}) or fill factor (FF), suggesting that grain boundaries in CZTSSe do not serve as recombination centers as is confirmed in a recent study,[55] but may scatter incident light and cause optical loss. To verify this hypothesis, we measured external quantum efficiency (EQE) spectra of three devices with increased amount of thiourea and indeed observed increased absorption in the red region of the solar spectrum (Figure 3B, dashed lines). Measurements at negative bias (−0.5 V) show only slight enhancement in charge collection (Figure 3B, solid lines), revealing that the observed loss is optical rather than electrical in nature.[56] Therefore, we conclude here that the enhancement in J_{SC} and efficiency in devices with larger grains is indeed due to reduced light scattering and improved light absorption. Further optimization of fabrication processes using the precursor with [tu]/[M] = 1.35 has led to highest total-area PCE of 6.52% without intentional sodium doping or antireflective coating (Figure S9).

DOI: 10.1021/jacs.5b05819
J. Am. Chem. Soc. 2015, 137, 11069−11075

Although the majority of this work is focused on the sol–gel-based fabrication, the principles we discussed above (Scheme 2) should apply to colloidal NCs as well. To confirm such universality, we demonstrate here that the amount and status of oleylamine (OAm) surfactants that cap colloidal CZTS NCs can also strongly affect their selenization processes. In previous work, we deposited and preannealed CZTS NCs under ambient atmosphere. OAm molecules undergo oxidative decomposition during such procedures, leaving behind relatively clean NC surfaces and thus facilitating the nucleation of Cu_xSe during selenization (Figure 4A).[35] In control

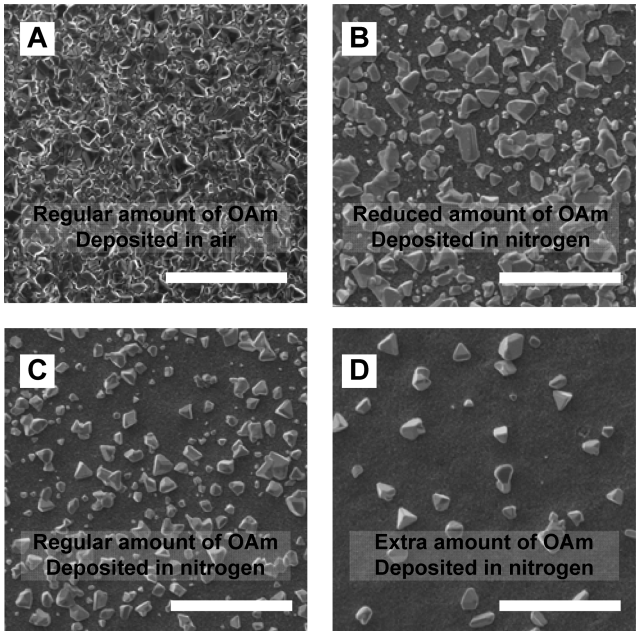

Figure 4. SEM images of selenized films from CZTS NCs capped with different amount of OAm ligands and deposited in air or inert atmosphere (scale bar = 10 μm).

experiments, we deposited NCs in exactly the same manner, except that films were deposited inside a nitrogen-fill glovebox. Selenization of these films result in isolated large grain layers (Figure 4C), as opposed to selenized film deposited in the presence of oxygen.[31] Such drastic difference clearly proves that the presence of largely intact OAm (boiling point 364 °C) inhibits the nucleation and growth of large crystals. Moreover, the presence of less or more amount of OAm leads to denser or scarcer large grains respectively compared to the standard condition (Figure 4B and 4D), further confirming that the solid–gas reactions can be effectively controlled via tuning the surface chemistry of NC precursors.

CONCLUSIONS

In summary, we have demonstrated the kinetic control of solid–gas reactions at nanoscale by manipulating the surface chemistry of both sol–gel NPs and colloidal NCs. Specifically, we have first identified that thiourea commonly used in sol–gel processes to fabricate CZTS transforms into melamine during film deposition, which serves as surface ligands for as-formed CZTS NPs. We further demonstrate that the presence of these surface ligands can significantly affect the nucleation step of the solid–gas reactions, which enables us to effectively control the selenization process during the fabrication of CZTSSe solar cells and achieve optimal film morphologies by fine-tuning the amount of surface ligands used. The enhancement of film morphologies and consequent light absorption allows us to achieve 6.5% efficiency of CZTSSe solar cells processed via a sol–gel process using nontoxic, low boiling point mixed solvents. We believe our discovery that the ligand of particles can significantly affect solid–gas reactions through manipulating the kinetics of nucleation is universal in solid-state chemistry and will trigger further research in both understanding the fundamentals of solid-state reactions at nanoscale and taking advantage of these reactions to fabricate crystalline thin film semiconductors with controlled morphologies and better device performances.

ASSOCIATED CONTENT

Supporting Information

The Supporting Information is available free of charge on the ACS Publications website at DOI: 10.1021/jacs.5b05819.

Evidences for the control of composition and stability of molecular inks, Raman spectra and XRD patterns of precursor and selenized films, optical images showing buildup and release of film stress, and device characteristics of the champion solar cell in this work. (PDF)

AUTHOR INFORMATION

Corresponding Author

*yangy@ucla.edu

Notes

The authors declare no competing financial interest.

ACKNOWLEDGMENTS

This work was financially supported by a grant from the National Science Foundation (Grant No.: ECCS-1202231, Program Director: Dr. George N. Maracas). The authors thank Prof. Wolfgang Schnick, Dr. W.-C. Hsu and Dr. T.-B. Song for valuable discussions. The authors also thank Dr. Robert Taylor for the SSNMR characterizations, Mr. H. Chen for the measurement using X-ray photoelectron spectrometer (XPS), Mr. W.-H. Chang for taking transmission electron microscope (TEM) images and Dr. Adam Stieg for the help with Kelvin probe force microscopy (KPFM).

REFERENCES

(1) Mitzi, D. B. *Solution Processing of Inorganic Materials*; John Wiley & Sons, Inc.: Hoboken, NJ, 2009.
(2) Dolzhnikov, D. S.; Zhang, H.; Jang, J.; Son, J. S.; Panthani, M. G.; Shibata, T.; Chattopadhyay, S.; Talapin, D. V. *Science* **2015**, *347*, 425.
(3) Nomura, K.; Ohta, H.; Takagi, A.; Kamiya, T.; Hirano, M.; Hosono, H. *Nature* **2004**, *432*, 488.
(4) Shimoda, T.; Matsuki, Y.; Furusawa, M.; Aoki, T.; Yudasaka, I.; Tanaka, H.; Iwasawa, H.; Wang, D.; Miyasaka, M.; Takeuchi, Y. *Nature* **2006**, *440*, 783.
(5) Lee, J.-S.; Kovalenko, M. V.; Huang, J.; Chung, D. S.; Talapin, D. V. *Nat. Nanotechnol.* **2011**, *6*, 348.
(6) Lee, J.-Y.; Connor, S. T.; Cui, Y.; Peumans, P. *Nano Lett.* **2008**, *8*, 689.
(7) Becerril, H. A.; Mao, J.; Liu, Z.; Stoltenberg, R. M.; Bao, Z.; Chen, Y. *ACS Nano* **2008**, *2*, 463.
(8) Faber, H.; Burkhardt, M.; Jedaa, A.; Kaelblein, D.; Klauk, H.; Halik, M. *Adv. Mater.* **2009**, *21*, 3099.
(9) Yun, J.; Cho, K.; Park, B.; Park, B. H.; Kim, S. *J. Mater. Chem.* **2009**, *19*, 2082.
(10) Qian, L.; Zheng, Y.; Xue, J.; Holloway, P. H. *Nat. Photonics* **2011**, *5*, 543.

DOI: 10.1021/jacs.5b05819
J. Am. Chem. Soc. 2015, 137, 11069–11075

(11) Dai, X.; Zhang, Z.; Jin, Y.; Niu, Y.; Cao, H.; Liang, X.; Chen, L.; Wang, J.; Peng, X. *Nature* **2014**, *515*, 96.
(12) Konstantatos, G.; Howard, I.; Fischer, A.; Hoogland, S.; Clifford, J.; Klem, E.; Levina, L.; Sargent, E. H. *Nature* **2006**, *442*, 180.
(13) Gur, I.; Fromer, N. A.; Geier, M. L.; Alivisatos, A. P. *Science* **2005**, *310*, 462.
(14) Tang, J.; Kemp, K. W.; Hoogland, S.; Jeong, K. S.; Liu, H.; Levina, L.; Furukawa, M.; Wang, X.; Debnath, R.; Cha, D.; Chou, K. W.; Fischer, A.; Amassian, A.; Asbury, J. B.; Sargent, E. H. *Nat. Mater.* **2011**, *10*, 765.
(15) Qin, P.; Tanaka, S.; Ito, S.; Tetreault, N.; Manabe, K.; Nishino, H.; Nazeeruddin, M. K.; Graetzel, M. *Nat. Commun.* **2014**, *5*, 3834.
(16) Hench, L. L.; West, J. K. *Chem. Rev.* **1990**, *90*, 33.
(17) Jiang, C.; Lee, J.-S.; Talapin, D. V. *J. Am. Chem. Soc.* **2012**, *134*, 5010.
(18) Kovalenko, M. V.; Manna, L.; Cabot, A.; Hens, Z.; Talapin, D. V.; Kagan, C. R.; Klimov, V. I.; Rogach, A. L.; Reiss, P.; Milliron, D. J.; Guyot-Sionnnest, P.; Konstantatos, G.; Parak, W. J.; Hyeon, T.; Korgel, B. A.; Murray, C. B.; Heiss, W. *ACS Nano* **2015**, *9*, 1012.
(19) Habas, S. E.; Platt, H. A. S.; van Hest, M. F. A. M.; Ginley, D. S. *Chem. Rev.* **2010**, *110*, 6571.
(20) Jasieniak, J.; MacDonald, B. I.; Watkins, S. E.; Mulvaney, P. *Nano Lett.* **2011**, *11*, 2856.
(21) Panthani, M. G.; Kurley, J. M.; Crisp, R. W.; Dietz, T. C.; Ezzyat, T.; Luther, J. M.; Talapin, D. V. *Nano Lett.* **2014**, *14*, 670.
(22) Mitzi, D. B.; Yuan, M.; Liu, W.; Kellock, A. J.; Chey, S. J.; Deline, V.; Schrott, A. G. *Adv. Mater.* **2008**, *20*, 3657.
(23) McLeod, S. M.; Hages, C. J.; Carter, N. J.; Agrawal, R. *Prog. Photovoltaics* **2015**, DOI: 10.1002/pip.2588.
(24) Todorov, T. K.; Reuter, K. B.; Mitzi, D. B. *Adv. Mater.* **2010**, *22*, E156.
(25) Guo, Q.; Ford, G. M.; Yang, W.-C.; Walker, B. C.; Stach, E. A.; Hillhouse, H. W.; Agrawal, R. *J. Am. Chem. Soc.* **2010**, *132*, 17384.
(26) Chang, J. A.; Im, S. H.; Lee, Y. H.; Kim, H.-j.; Lim, C.-S.; Heo, J. H.; Seok, S. I. *Nano Lett.* **2012**, *12*, 1863.
(27) Zhou, Y.; Leng, M.; Xia, Z.; Zhong, J.; Song, H.; Liu, X.; Yang, B.; Zhang, J.; Chen, J.; Zhou, K.; Han, J.; Cheng, Y.; Tang, J. *Adv. Energy Mater.* **2014**, *4*, 1301846.
(28) Chuang, C.-H. M.; Brown, P. R.; Bulović, V.; Bawendi, M. G. *Nat. Mater.* **2014**, *13*, 796.
(29) Kim, J.; Hiroi, H.; Todorov, T. K.; Gunawan, O.; Kuwahara, M.; Gokmen, T.; Nair, D.; Hopstaken, M.; Shin, B.; Lee, Y. S.; Wang, W.; Sugimoto, H.; Mitzi, D. B. *Adv. Mater.* **2014**, *26*, 7427.
(30) Mainz, R.; Walker, B. C.; Schmidt, S. S.; Zander, O.; Weber, A.; Rodriguez-Alvarez, H.; Just, J.; Klaus, M.; Agrawal, R.; Unold, T. *Phys. Chem. Chem. Phys.* **2013**, *15*, 18281.
(31) Guo, Q.; Caspar, J. V.; Roelofs, K. E.; Subramoney, S.; Rosenfeld, H. D. *Chem. Mater.* **2014**, *26*, 5664.
(32) Embden, J. v.; Chesman, A. S. R.; Gaspera, E. D.; Duffy, N. W.; Watkins, S. E.; Jasieniak, J. J. *J. Am. Chem. Soc.* **2014**, *136*, 5237.
(33) Jiang, C.; Liu, W.; Talapin, D. V. *Chem. Mater.* **2014**, *26*, 4038−4043.
(34) Carrete, A.; Shavel, A.; Fontane, X.; Montserrat, J.; Fan, J.; Ibanez, M.; Saucedo, E.; Perez-Rodríguez, A.; Cabot, A. *J. Am. Chem. Soc.* **2013**, *135*, 15982.
(35) Hsu, W.-C.; Zhou, H.; Luo, S.; Song, T.-B.; Hsieh, Y.-T.; Duan, H.-S.; Ye, S.; Yang, W.; Hsu, C.-J.; Jiang, C.; Bob, B.; Yang, Y. *ACS Nano* **2014**, *8*, 9164.
(36) Su, Z.; Sun, K.; Han, Z.; Cui, H.; Liu, F.; Lai, Y.; Li, J.; Hao, X.; Green, M. A.; Liu, Y. *J. Mater. Chem. A* **2014**, *2*, 500.
(37) Yao, Y.; Hou, J.; Xu, Z.; Li, G.; Yang, Y. *Adv. Funct. Mater.* **2008**, *18*, 1783.
(38) Shevchenko, E. V.; Talapin, D. V.; Kotov, N. A.; O'Brien, S.; Murray, C. B. *Nature* **2006**, *439*, 55.
(39) Madarasz, J.; Bombicz, P.; Okuya, M.; Kaneko, S. *Solid State Ionics* **2001**, *141−142*, 439.
(40) Bowmaker, G. A.; Hanna, J. V.; Pakawatchai, C.; Skelton, B. W.; Thanyasirikul, Y.; White, A. H. *Inorg. Chem.* **2009**, *48*, 350.
(41) Zaberca, O.; Oftinger, F.; Chane-Ching, J. Y.; Datas, L.; Lafond, A.; Puech, P.; Balocchi, A.; Lagarde, D.; Marie, X. *Nanotechnology* **2012**, *23*, 185402.
(42) Krunksa, M.; Miklib, V.; Bijakinaa, O.; Rebanea, H.; Merec, A.; Varemaa, T.; Mellikova, E. *Thin Solid Films* **2000**, *361−362*, 61.
(43) Wang, S.; Gao, Q.; Wang, J. *J. Phys. Chem. B* **2005**, *109*, 17281.
(44) Braml, N. E.; Sattler, A.; Schnick, W. *Chem. - Eur. J.* **2012**, *18*, 1811.
(45) Lotsch, B. V.; Schnick, W. *Chem. - Eur. J.* **2007**, *13*, 4956.
(46) Juergens, B.; Irran, E.; Senker, J.; Kroll, P.; Mueller, H.; Schnick, W. *J. Am. Chem. Soc.* **2003**, *125*, 10288.
(47) Rozhenko, A. B.; Trachevsky, V. V. *Phosphorus, Sulfur Silicon Relat. Elem.* **2009**, *184*, 1386.
(48) Damodaran, K.; Sanjayan, G. J.; Rajamohanan, P. R.; Ganapathy, S.; Ganesh, K. N. *Org. Lett.* **2001**, *3*, 1921.
(49) Sattler, A.; Pagano, S.; Zeuner, M.; Zurawski, A.; Gunzelmann, D.; Senker, J.; Mueller-Buschbaum, K.; Schnick, W. *Chem. - Eur. J.* **2009**, *15*, 13161.
(50) Fella, C. M.; Uhl, A. R.; Hammond, C.; Hermans, I.; Romanyuk, Y. E.; Tiwari, A. N. *J. Alloys Compd.* **2013**, *567*, 102.
(51) Chernomordik, B. D.; Béland, A. l. E.; Deng, D. D.; Francis, L. F.; Aydil, E. S. *Chem. Mater.* **2014**, *26*, 3191.
(52) Yin, X.; Tang, C.; Sun, L.; Shen, Z.; Gong, H. *Chem. Mater.* **2014**, *26*, 2005.
(53) Wu, W.; Cao, Y.; Caspar, J. V.; Guo, Q.; Johnson, L. K.; Malajovich, I.; Rosenfeld, H. D.; Choudhury, K. R. *J. Mater. Chem. C* **2014**, *2*, 3777.
(54) Shin, B.; Zhu, Y.; Bojarczuk, N. A.; Chey, S. J.; Guha, S. *Appl. Phys. Lett.* **2012**, *101*, 053903.
(55) Gershon, T.; Shin, B.; Bojarczuk, N.; Hopstaken, M.; Mitzi, D. B.; Guha, S. *Adv. Energy Mater.* **2015**, *5*, 1400849.
(56) Hegedus, S. S.; Shafarman, W. N. *Prog. Photovoltaics* **2004**, *12*, 155.

DOI: 10.1021/jacs.5b05819
J. Am. Chem. Soc. 2015, 137, 11069−11075